Journal of Alloys and Compounds 971 (2024) 172712

Contents lists available at ScienceDirect

Journal of Alloys and Compounds

journal homepage: www.elsevier.com/locate/jalcom

Detailed studies of superconducting properties of $Y_2Pd_{1.25}Ge_{2.75}$

Hanna Świątek [a,b], Szymon Królak [a,b], Leszek Litzbarski [a,b,c], Igor Oshchapovsky [a,b,d], Michał J. Winiarski [a,b], Tomasz Klimczuk [a,b,*]

[a] Faculty of Applied Physics and Mathematics, Gdańsk University of Technology, Narutowicza 11/12, 80-233 Gdansk, Poland
[b] Advanced Materials Center, Gdańsk University of Technology, Narutowicza 11/12, 80-233 Gdansk, Poland
[c] Faculty of Electrical and Control Engineering, Gdansk University of Technology, Narutowicza 11/12, 80-233 Gdansk, Poland
[d] Department of Inorganic Chemistry, Ivan Franko National University of Lviv, Kyryla i Mefodiya Str. 6, 79005 Lviv, Ukraine

ARTICLE INFO

Keywords:
Intermetallic compound
AlB2 related crystal structure
Superconductivity

ABSTRACT

We report a successful synthesis of a high-purity intermetallic germanide $Y_2Pd_{1.25}Ge_{2.75}$, crystallizing in the disordered variant of the AlB_2-type structure. A single-phase sample was obtained via arc-melting by deliberately tuning the composition out of the ideal 2:1:3 ratio. Specific heat, electrical resistivity and magnetization measurements show that the compound is a weakly-coupled ($\lambda_{e\text{-}p} = 0.58$) type-II superconductor with a superconducting transition at $T_c = 2.72$ K. Additional magnetization measurements conducted under pressure up to 0.55 GPa show suppression of T_c, at a rate of -0.17 K/GPa. Electronic structure calculations reveal the deep similarity between $Y_2Pd_{1.25}Ge_{2.75}$ and other AlB_2-type germanide superconductors, especially the ordered YGa_2 phase.

1. Introduction

The discovery of superconductivity in MgB_2 with a surprisingly high $T_c = 39$ K [1] was crucial for the technical applications of superconductors [2–4]. Moreover, MgB_2 is also known to exhibit a two-band superconductivity, which is in contrast to its relatively simple crystal structure (a hexagonal AlB_2-type) [5]. This crystal structure can be represented as parallel honeycomb layers of B atoms, separated by a triangular Mg sublattice. Substitution of Al and B atoms produces a large family of binary compounds with REX_2 or RET_2 a stoichiometry, where RE is a rare earth metal, alkali metal or actinoid, T is a transition metal and X is a main group element [6]. In the case of ternary RE_2TX_3 compounds, there are two possible variants of the AlB_2-derived structure, i.e. an ordered and a disordered one, which can be distinguished by the c/a ratio [7]. The disordered nature of this crystal structure favors the formation of a spin glass-like state, which has been observed for many reported RE_2TX_3 compounds, e.g. Nd_2PtGe_3 [8], Ce_2CuGe_3 [9] and Er_2NiSi_3 [10]. The members of the RE_2TX_3 family with a non-magnetic RE element (Sc, Y, La and Lu) reveal superconducting ground state, e.g. Y_2PtGe_3 ($T_c = 3.3$ K) [11], and La_2NiGe3 ($T_c \approx 0.45$ K) [12]. It should be noted that many of the RE_2TX_3 compounds cannot be synthetized as a single phase with a nominal 2–1–3 stoichiometry, even when thermal annealing is employed. There are two known remedies for this problem: introducing vacancies in the honeycomb layers by modifying the stoichiometry to obtain $RE_2T_{1-x}X_{3-y}$ [13–15] or adjusting the composition of this sublattice in order to synthetize $RE_2T_{1+x}Ge_{3-x}$ compounds [16–18].

The intermetallic compound Y_2PdGe_3 was the first reported member of RE_2TX_3 series revealing superconducting properties [19]. However, the samples studied by authors of [19] were contaminated with a parasitic phase, which could affect the experimental results. Despite this fact, it was a significant contribution to the discussion about the origin of superconductivity in the isostructural MgB_2 [20]. Furthermore, Y_2PdGe_3 was a promising research subject for the chemical substitution experiments, which in the case of MgB_2 are limited due to volatility of Mg. An example of such an experiment was the replacement of Ge atoms with Si and C in a honeycomb sublattice of Y_2PdGe_3, described in ref. [21]. An arc melting technique was used to obtain intermetallic compounds: Y_2PdGe_3, Y_2PdSi_3, $Y_2PdSi_{2.25}C_{0.75}$, Y_2PdSi_2C and $Y_2PdSi_{1.5}C_{1.5}$. Analysis of powder X-ray diffraction (pXRD) data indicated that all of the investigated samples crystallize in the disordered variant of AlB_2 aristotype, but only Y_2PdSi_3 was found to be single–phase. The physical properties measurements revealed that the aforementioned compounds are superconductors (with the exception of Y_2PdSi_3). The hypothesis of a correlation between T_c and the molar mass of the elements occupying the honeycomb layers was not confirmed, and instead a dependence on

* Corresponding author at: Faculty of Applied Physics and Mathematics, Gdańsk University of Technology, Narutowicza 11/12, 80-233 Gdansk, Poland.
E-mail address: tomasz.klimczuk@pg.edu.pl (T. Klimczuk).

https://doi.org/10.1016/j.jallcom.2023.172712
Received 31 July 2023; Received in revised form 25 October 2023; Accepted 29 October 2023
Available online 31 October 2023

the parameter a was observed [21].

The increase of the lattice parameter a in the AlB_2-type structure causes a shrinkage of the c lattice parameter and consequently an increase in the strength of the interactions between the neighboring RE layers. It is consistent with the results presented in [22] about the interplay between Debye temperature and the electron-phonon coupling constant in the $Y_2PdGe_{3-x}Si_x$ series. The lattice parameter a increases with Si concentration, while the lattice constant c decreases. A correlation between the honeycomb sublattice contraction and a decrease in T_c is observed, which may be a result of a variation in the electron-phonon coupling. The influence of substitution of Pd by Pt in the Y_2PdGe_3 compound was studied by K.K. Iyer and E.V. Sampathkumaran [23]. It was found that increasing the Pd concentration causes an increase in the lattice parameter a and a decrease in c, while the volume of the unit cell remains almost constant. This phenomenon is in accordance with the empirical Vegard's law [24], which means that the hexagonal layers behave similarly to a solid solution. Replacement of Pd atoms by Pt resulted in a decrease in T_c, possibly due to changing chemical pressure effects caused by the difference in atomic radius between Pt and Pd [25,26].

In this paper we report the successful synthesis of a chemically pure intermetallic compound Y_2PdGe_3. A single-phase material can be obtained by deliberately varying the ratio of Pd to Ge, resulting in a nominal stoichiometry of $Y_2Pd_{1.25}Ge_{2.75}$. The paper describes a detailed characterization of its crystal structure and the results of physical properties including magnetization, specific heat and electrical resistivity measurements. For the first time, the results of magnetization measurements carried out under pressure are presented and discussed.

2. Materials and methods

A series of polycrystalline samples of $Y_2Pd_{1+x}Ge_{3-x}$ (x = 0 – 0.35) intermetallic compounds were obtained by the arc melting technique from appropriate amounts of high-purity constituent elements, i.e. Y (99.9%, Onyxmet), Pd (99.5%, Alfa Aesar) and Ge (99.999%, Alfa Aesar). The synthesis procedure was performed in an inert atmosphere (Zr-gettered high purity Ar) employing the arc furnace MAM-1 GmbH Edmund Bühler. In order to improve the homogeneity of the samples, ingots were flipped and re-melted several times. The final alloying level of the synthetized materials was close to the assumed composition, which was confirmed by negligible mass losses during the melting process (~0.5%). No further thermal treatment was performed due to secondary RET_2Ge_2 phase appearing as a result of prolonged annealing, as previously observed for Tb_2PdGe_3 [16]. The phase purity was checked by powder X-ray diffraction (pXRD), using Bruker D2Phaser diffractometer equipped with XE-T detector (Cu-Kα radiation). Structural parameters of studied samples were obtained by Rietveld analysis of the gathered pXRD data carried out with Jana2006 software [27]. The samples were also examined by energy-dispersive X-ray spectroscopy (EDX) using a scanning electron microscope FEI Quanta FEG 250 to confirm their chemical composition. Magnetic properties were investigated using a Quantum Design Physical Property Measurement System (PPMS) with a vibrating sample magnetometer (VSM) option. The DC magnetization measurements were carried out in both zero field cooling (ZFC) and field cooling (FC) modes in a temperature range 2–300 K at different applied magnetic fields. Heat capacity data was collected using a standard thermal relaxation technique, with and without an external magnetic field. The electrical resistivity measurements were performed using a four probe technique with an applied current of 5 mA. Electrical contacts were made by spot-welding platinum wires ($\phi = 50$ μm) on the polished surface of the samples. This method provides excellent electrical contact quality with contact resistance below the value measurable by a typical ohmmeter (less than 0.5 Ω). High pressure magnetization measurements were performed using a piston-cylinder type copper-beryllium bronze cell (HMD, Japan) compatible with the PPMS VSM option. The Daphne 7373 (Idemitsu, Japan) oil was used as a pressure transmitting medium. The sample was packed together with a small piece (~2 mg) of high purity lead wire which was employed as a manometer. The cell pressure was calculated based on the pressure coefficient of the critical temperature for Pb from ref [28].

Density functional theory (DFT) calculations of the electronic structure of $Y_2Pd_{1-x}Ge_{3-x}$ and its Ni- and Pt- bearing analogues were performed using the Korringa-Kohn-Rostocker (KKR) method within the Atomic Sphere Approximation (ASA) and employing the Coherent Potential Approximation (CPA) to address the atomic disorder. Calculations were done using the Munich SPR-KKR 8.6 code [29,59] and the xband 6.3 graphical user interface. The Perdew-Burke-Ernzerhof generalized gradient approximation (PBE GGA)[30] of the exchange-correlation potential was used.

3. Results and discussion

The purity of all the samples was checked by the powder x-ray diffraction (pXRD) analysis. The sample with the $Y_2Pd_{1.25}Ge_{2.75}$ composition was selected for further characterization as it did not contain the parasitic 1:2:2 phase that was present in the other samples. The EDX analysis of the sample showed that the composition of the pellet (34:21:45) is within an error of the nominal composition. The pXRD pattern is presented in Fig. 1. The hexagonal P6/mmm structure type was refined by the Rietveld refinement of the pXRD pattern with the lattice parameters $a = 4.2217$ (1) Å and $c = 3.9340(1)$ Å. There are two structural studies of the "Y_2PdGe_3" reported in the literature. For the isotypical Y_2PdGe_3 alloy Majumdar, et al. obtained $a = 4.192$ Å, $c = 4.000$ Å [19]. For the samples with the nominal compositions $Y_2Pd_{1.5}Ge_{2.5}$ and $Y_2Pd_{0.8}Ge_{3.2}$ the refined parameters are: $a = 4.270$ Å, $c = 3.803$ Å and $a = 4.146$ Å, $c = 4.031$ Å, respectively [31]. It is important to note that the diffraction patterns reported in [19] and [31] show significant amounts of a secondary phase, whereas the sample studied here, with a nominal stoichiometry of $Y_2Pd_{1.25}Ge_{2.75}$, is chemically pure. Despite these differences, there is a clear tendency for the a parameter to increase and the c parameter to decrease with increasing Pd/Ge ratio – see Table 1.

The pXRD pattern reveals an anisotropic broadening and unusual asymmetries of the diffraction reflections, similar to those observed in the other related R_2TGe_3 compounds [16–18]. Many of the pXRD reflections were smeared towards higher angles, which was opposite to the asymmetry, caused by the instrumental profiles of the diffractometers. It was therefore necessary to describe these features using anisotropic

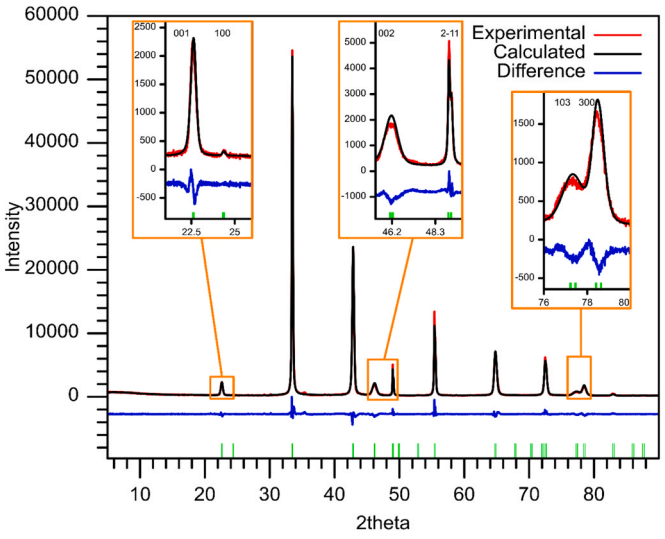

Fig. 1. Rietveld refinement using powder XRD data for alloy $Y_2Pd_{1.25}Ge_{2.75}$ in space group *P6/mmm* with split left/right profile and anisotropic size/strain broadening.

Table 1
Reported lattice parameters for different $Y_2Pd_{1+x}Ge_{3-x}$.

Nominal stoichiometry	*Pd/Ge*	a (Å)	c (Å)	Ref.
$Y_2Pd_{0.8}Ge_{3.2}$	0.25	4.146	4.031	[31]
Y_2PdGe_3	0.33	4.192	4.000	[19]
$Y_2Pd_{1.25}Ge_{2.75}$	0.45	4.2217	3.934	this work
$Y_2Pd_{1.5}Ge_{2.5}$	0.6	4.270	3.803	[31]

size/strain broadening and split left/right profile parameters. Several possible supercells and distorted unit cells were tested and a conventional hexagonal unit cell was preferred, its symmetry being checked by the Superflip program [32]. The final Rietveld refinement also considered the surface roughness, preferred orientation and isotropic thermal displacement parameters of the atoms. Taking into account the relatively small differences between the atomic numbers (and thus the X-ray scattering factor) of Y, Pd, and Ge, the site occupation factors for the mixed Pd/Ge 2*d* site were fixed to the nominal values (0.3125 and 0.6875, respectively) and the isotropic displacement parameters of Pd and Ge were constrained to be equal. Further details of the crystal structure analysis are given in Supplementary Information.

The zero-field electrical resistivity ρ(T) for $Y_2Pd_{1.25}Ge_{2.75}$ in the full temperature range 1.8 – 310 K is shown in a main panel of Fig. 2. As the temperature is lowered, the resistivity decreases ($d\rho/dT > 0$) as expected for metallic materials, although the temperature dependence is marginal. The calculated residual resistivity ratio (RRR = ρ(300 K)/ ρ_0) is close to 1.1. A low value of RRR is due to the polycrystalline nature of the sample and the expected structural disorder (site Pd/Ge mixing) in $Y_2Pd_{1.25}Ge_{2.75}$.

In the low temperature region a sharp drop in resistivity is observed, associated with the onset of superconductivity. The critical temperature T_c, determined as a midpoint of the transition, is equal to 3.27 K. This value is slightly higher than that previously reported for the stoichiometric composition Y_2PdGe_3, where T_c = 3 K [20] and is very close to the 3.3 K reported for Y_2PtGe_3 [11]. Just above the superconducting transition a slight upturn of ρ(T) is observed. This feature has not been previously reported for the AlB_2-type ternary germanide family members. However, the presence of a resistivity peak close to the transition temperature is a common feature for inhomogeneous materials and has previously been observed for $Pr_{2-x}Ce_xCuO_4$[33], $Nd_{2-x}Ce_xCuO_{4-y}$[34] and TaP [35]. The inset shows the isothermal magnetic field dependence of the resistivity, with the ρ(μ_0H) data collected at 2 K. The upper critical field at this temperature is estimated to be μ_0H_{c2} = 1.3 T (see two solid lines).

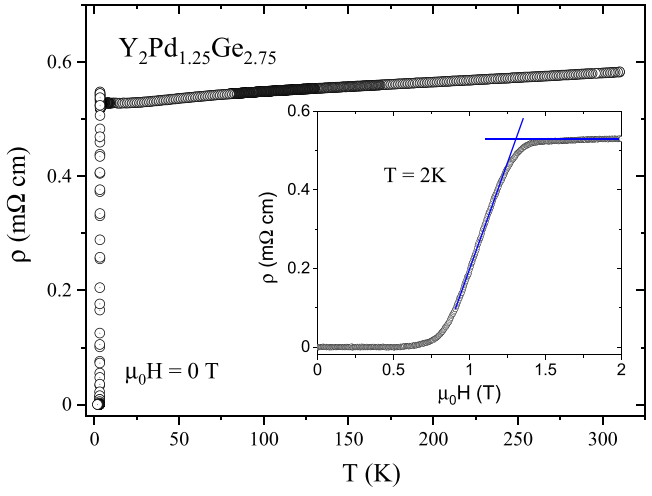

Fig. 2. Zero-field temperature dependence of resistivity. Inset: field-dependent resistivity measured at 2 K, with the line intersection marking the estimated upper critical field μ_0H_{c2}(2 K) = 1.3 T.

The superconducting transition has also been analyzed in a range of applied magnetic fields (μ_0H). Fig. 3 presents temperature dependent ρ(T) for μ_0H = 0 – 0.8 T. Increasing the magnetic field shifts the transition to lower temperatures. The transition also broadens considerably, from ΔT = 0.25 K for the zero-field measurement to around ΔT = 0.85 K when the highest field (0.8 T) is applied. A close-up of the ρ(T) anomaly is shown in the lower panel. The anomaly is magnetic field dependent, and the size of the peak appears to decrease with higher magnetic fields. In addition, for the lowest fields, as the temperature is lowered, we observe first a slight dip, followed by a sharp upturn, leading directly afterwards to the superconducting transition. This part of the anomaly is no longer observed for fields above μ_0H = 20 mT and is of unknown origin. For the magnetic fields above 0.8 T, the superconducting transition is fully suppressed.

The upper critical field values μ_0H_{c2}(T) were estimated as the midpoints of the ρ(T) transitions under different fields and are plotted in Fig. 4. The data were fitted using the formula proposed by Micnas et al. [36]: $H_{c2}(T) = H_{c2}(0)\left[1 - \left(\frac{T}{T_c}\right)^{3/2}\right]^{3/2}$, which has previously been used for superconductors exhibiting positive curvature of H_{c2}(T) near T_c [37, 38], including another AlB_2-type ternary compound $BaCu_xSi_{2-x}$ [39]. The fit gives $\mu_0H_{c2}(0)$ = 2.94(5) T. A blue star indicates the additional point estimated from the T = 2 K isothermal ρ(H) measurement (see inset of Fig. 2).

The temperature dependence of the specific heat C_p(T), in the full temperature range T = 1.9 – 300 K in zero magnetic field, is presented in Fig. 5. At room temperature C_p reaches the expected Dulong-Petit limit, determined as 3nR = 150 J mol^{-1} K^{-1}, where the number of atoms per formula unit n = 6 and the gas constant R = 8.31 J mol^{-1} K^{-1}. Fig. 6 shows a closer look at the low temperature region, below 5 K. The C_p data were collected under the applied magnetic field of μ_0H = 0.9 T, which exceeds the upper critical field for $Y_2Pd_{1.25}Ge_{2.75}$. The plot is presented as C_p/T vs T^2 to show the low-T Debye relation ($C_{ph} \sim T^3$). The experimental points were fitted in the temperature range of T = 2.3 – 4.2 K using the formula $C_p/T = \gamma + \beta T^2$, where the former term is the Sommerfeld coefficient related to the electronic contribution to the heat

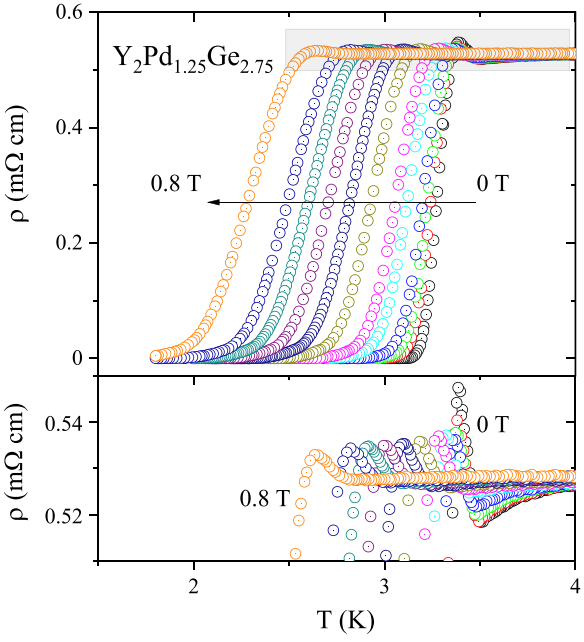

Fig. 3. Change of resistivity in the low-temperature region with applied magnetic fields in the range of 0–0.8 T (0, 5 mT, 10 mT, 20 mT, 60 mT, 0.1 T, 0.2 T, 0.3 T, 0.4 T, 0.5 T, 0.6 T, 0.8 T). Lower panel: a close-up of resistivity peaks preceding the onset of superconductivity.

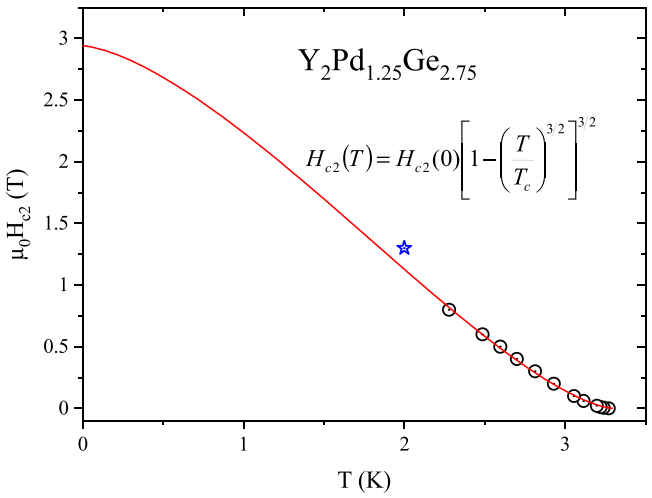

Fig. 4. Temperature dependence of the upper critical field determined from resistivity measurements (marked with black circles) and the point estimated from ρ(μ$_0$H) measurement (marked with a blue star).

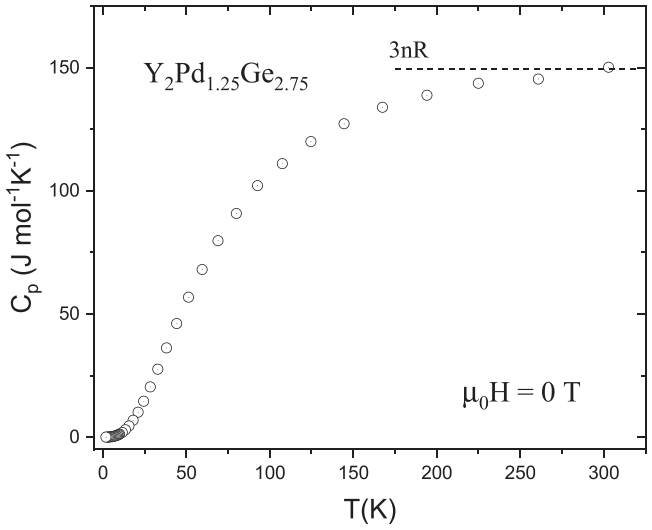

Fig. 5. Zero-field specific heat in the full temperature range.

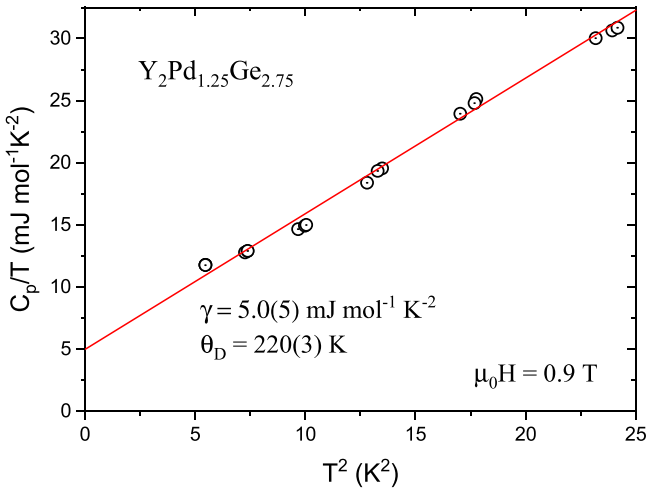

Fig. 6. Normal-state C_p/T vs T^2 in the low temperature region measured at μ_0H = 0.9 T. The red line corresponds to a linear fit used to determine electronic and phonon contributions to specific heat.

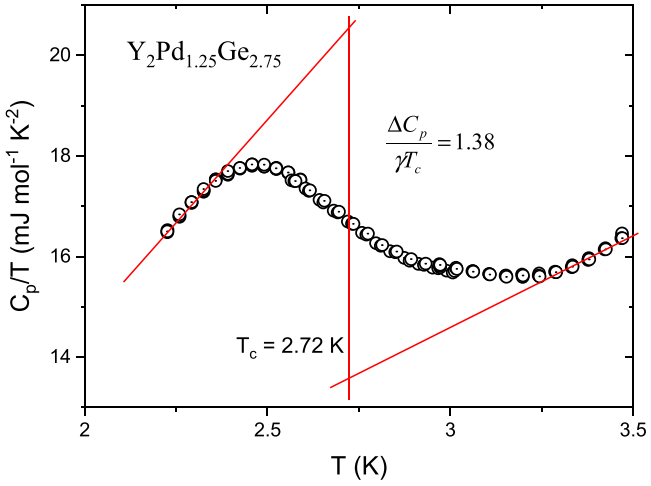

Fig. 7. The specific heat anomaly presented as C_p/T vs T in zero-field. The red lines represent the equal-entropy construction used to determine the normalized specific heat jump.

capacity (γT) and the latter term represents the phonon specific component (βT^3). The fit yielded the values γ = 5.0(5) mJ mol^{-1} K^{-2} and β = 1.09(4) mJ mol^{-1} K^{-4}. Knowing the value of the β coefficient, the Debye temperature can be calculated using the relationship:

$$\theta_D = \left(\frac{12\pi^4 nR}{5\beta}\right)^{1/3}.$$

The calculation resulted in θ_D = 220(3) K. Both the Sommerfeld coefficient and the Debye temperature are significantly higher than those reported for the stoichiometric Y_2PdGe_3, where γ = 2.5 mJ mol^{-1} K^{-2} and θ_D = 130 K [20].

The specific heat jump at the transition temperature in zero magnetic field is presented in Fig. 7 as C_p/T vs T. The superconducting transition estimated by this method is T_c = 2.7 K and is about 0.5 K lower than the value obtained from the resistivity measurement, likely due to compositional and structural inhomogeneity leading to the occurrence of filamentary superconducting paths, e.g. at grain boundaries [40]. The transition is relatively broad, which may be due to structural disorder or thermal strain in the sample. In addition to Pd-Ge atomic mixing, we have previously observed that $R_2Pd_{1+x}Ge_{3-x}$ compounds often exhibit significant anisotropic broadening, which may be due to the presence of stacking faults [16–18]. However, it is worth noting that such a broad transition was also observed in the isostructural compound YGa_2, for which no significant atomic disorder was found [41].

Knowing the Sommerfeld parameter and using the equal entropy construction (marked with red lines), the normalized specific heat jump was determined to be $\Delta C_p/\gamma T_c$ = 1.38. The value is very close to the 1.43 predicted by BCS theory for weakly coupled superconductors.

The critical temperature and the calculated Debye temperature can be used to calculate the electron-phonon coupling parameter $\lambda_{e\text{-}p}$, according to the inverted McMillan formula [42].

$$\lambda_{e-p} = \frac{1.04 + \mu^* \ln(\theta_D/1.45T_c)}{(1-0.62\mu^*)\ln(\theta_D/1.45T_c) - 1.04}$$

where μ * is the Coulomb pseudopotential parameter, which typically takes a value in the range 0.10–0.15. Using μ * = 0.13, T_c = 2.7 K and θ_D = 220 K, the value $\lambda_{e\text{-}p}$ = 0.58 was obtained, indicating weak coupling. Having calculated this parameter and using the previously obtained value of the Sommerfeld coefficient γ, the non-interacting density of states at the Fermi level DOS(E_F) could be calculated according to the formula:

$$DOS(E_F) = \frac{3\gamma}{\pi^2 k_B^2 (1+\lambda_{e-p})}$$

where k_B is the Boltzmann constant. It was estimated to be DOS(E_F) = 1.33 states eV^{-1} per formula unit (f.u.).

To further characterize the superconducting properties, dc volume magnetic susceptibility ($\chi_v = M_V/H$) was measured in zero field-cooled (ZFC) and field-cooled (FC) modes, in the temperature range of 1.9 – 5 K, under an applied magnetic field of 10 Oe. Fig. 8 shows the volume magnetic susceptibility χ_v as a function of temperature.

The strong diamagnetic signal and the divergence of the ZFC and FC curves below 3 K further confirm superconductivity. The data have been corrected for the demagnetization effect according to the $-4\pi\chi_v = \frac{1}{1-N}$ relation, with a demagnetization factor N = 0.16 estimated from subsequent isothermal measurements. At the lowest temperatures the ZFC curve approaches the value of − 1, indicating an almost 100% shielding fraction. The small Meissner fraction in the FC data is expected for polycrystalline materials. The T_c determined from this measurement, as the intersection of the extrapolated normal state data with the line defined by the maximum slope of the χ_v ZFC curve [43], is 2.87 K, in agreement with the value obtained from the specific heat results.

In order to determine the lower critical field $H_{c1}(0)$, a series of isothermal low field magnetization measurements were carried out, for the temperatures ranging from T = 1.9 to T = 2.8 K (below T_c) – see the inset of Fig. 8. For each temperature, a magnetic field value corresponding to the point of deviation from the initial linear behavior of the Mv(H) curve was determined. The points obtained are plotted in the main panel of Fig. 9, with an additional zero field point obtained from the resistivity measurement. The data were then fitted using the formula:

$$H_{c1}^*(T) = H_{c1}^*(0)\left[1-\left(\frac{T}{T_c}\right)^2\right].$$

The value obtained was equal to 23(1) Oe, and when corrected for the demagnetization factor yielded $H_{c1}(0)$ = 27 Oe. This result is an order of magnitude lower than that reported for Y_2PdGe_3, where H_{c1}(1.7 K) = 400 Oe [20], and is closer to the H_{c1}(1.8 K) = 50 Oe obtained for Y_2PtGe_3 [11].

Knowing both the H_{c1} and H_{c2} values, two other important superconducting parameters can be estimated. The coherence length ξ_{GL} can be calculated from the Ginzburg-Landau formula $H_{c2} = \phi_0/2\pi\ \xi_{GL}^2$, where Φ_0 is the quantum flux. Using $\mu_0 H_{c2}(0)$ = 2.94 T gives $\xi_{GL}(0)$ = 106 Å. Next, the superconducting penetration depth λ_{GL} can be

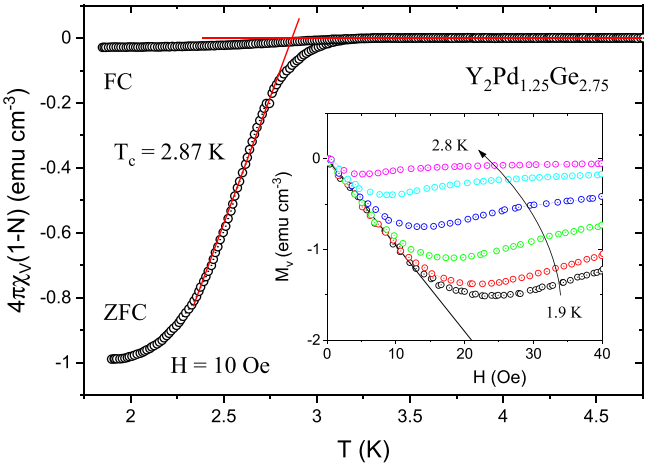

Fig. 8. Zero-field-cooled (ZFC) and field-cooled (FC) volume magnetic susceptibility measured at 10 Oe. Inset: field-dependent magnetization curves collected at various temperatures (1.9 K, 2 K, 2.4 K, 2.6 K and 2.8 K).

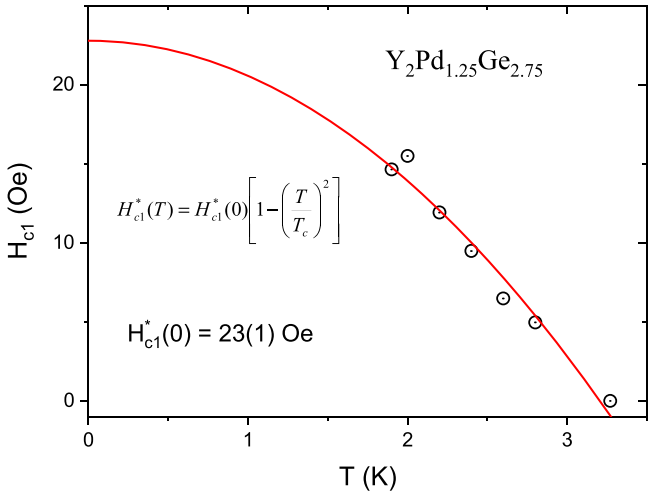

Fig. 9. Temperature dependence of H_{c1}^* determined from magnetization measurements.

obtained from the relation:

$$H_{c1} = \frac{\phi_0}{4\pi\lambda_{GL}^2}\ln\frac{\lambda_{GL}}{\xi_{GL}}.$$

The calculations yield two possible solutions to this equation, $\lambda_{GL}(0)$ = 4820 Å and $\lambda_{GL}(0)$ = 182 Å. However, the latter result leads to an unreasonably low value of the Ginzburg-Landau parameter calculated as $\kappa_{GL} = \lambda_{GL}/\xi_{GL}$, equal to 1.7. On the other hand, $\lambda_{GL}(0)$ = 4820 Å gives κ_{GL} = 45 > >$1/\sqrt{2}$, firmly indicating type-II superconductivity, in line with the observed M(H) curves shown in the inset of Fig. 8. Thus, the values $\lambda_{GL}(0)$ = 4820 Å and κ_{GL} = 45 are accepted as more probable. Having kappa we can calculate the thermodynamic critical field using the equation $H_{c1}H_{c2} = H_c^2 \ln\kappa$, obtaining a value of 46 mT. The H_c can also be estimated according to the relation $\frac{\mu_0 H_c^2(0)}{2} = \iint (C_N - C_{SC})/T\ dT$, using the difference of the specific heat data collected for the zero field and the normal state (0.9 T). The value estimated by this method is 23 mT, giving an order of magnitude consistent with the previously obtained result and confirming the validity of chosen λ_{GL}.

The magnetization measurements were also carried out under a range of applied pressures, up to 0.55 GPa. The inset of Fig. 10 shows the collected magnetization curves at the temperatures surrounding the superconducting transition. The slight discrepancy between the critical

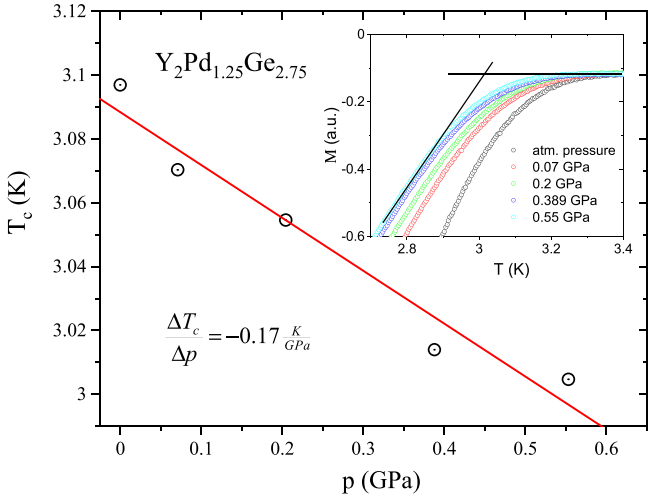

Fig. 10. Pressure dependence of critical temperature at 5 Oe. The red line represents a linear fit. Inset: temperature-dependent magnetization curves.

temperature values obtained from the magnetization curves at ambient pressure, with and without the use of the pressure cell, is due to the fact that the measurements were performed at 5 and 10 Oe respectively.

As the pressure is increased, the transition moves towards lower temperature. The T_c values, determined in the same way as $\chi_v(T)$ in the previous section, are presented in the main panel of Fig. 10. A linear fit of the collected data points gives a rate of change of $dT_c/dp = -0.17$ K/GPa. The pressure coefficient is similar to that reported for SrAlSi crystallizing in an AlB_2-related structure ($dT_c/dp = -0.12$ K/GPa) [44,45] and twice lower than that reported for the Heusler-type superconductors, e.g. $dT_c/dp = -0.23$ K/GPa for $MgPd_2Sb$ [46].

A complete set of the characteristic parameters for $Y_2Pd_{1.25}Ge_{2.75}$ is summarized in Table 2.

The results of the electronic structure calculations are shown in Figs. 11 and 12. The electronic density of states (DOS) at the Fermi level E_F is not significantly affected by tuning the Pd:Ge ratio from 1:3–1.25:2.75 (Fig. 11(a)). The calculated DOS(E_F) = 1.37 states/eV/f. u. is in good agreement with the non-interacting value estimated using the Sommerfeld coefficient and the electron-phonon coupling coefficient (see Table 2).

The DOS of the isostructural superconductors YGa_2, Y_2NiGe_3, and Y_2PtGe_3 (Fig. 11(b,c,d,), respectively) shows a similar peak above the E_F, which is mainly contributed by the Y *d* states. The position of a peak below the E_F varies between the Ni-, Pd-, and Pt-bearing analogues. Only in the case of Y_2NiGe_3 (Fig. 11(c)) is the Ni *d* orbital contribution dominant over Y and Ge.

Fig. 12 shows the Bloch spectral function (BSF) for $Y_2Pd_{1.25}Ge_{2.75}$ and its analogues. The BSF can be used to study the band structure of a disordered solid, for which the Bloch eigenstates are not well defined due to the broken periodicity [47]. A striking similarity of the Bloch spectral function of $Y_2Pd_{1.25}Ge_{2.75}$ and the band structure of the ordered isostructural YGa_2 can be rationalized by considering the valence electron count (VEC) and the electronic DOS (Fig. 11(a) and (b)). YGa_2 consists of $3 + 2{\cdot}3 = 9$ valence electrons per cell. The unit cell of $Y_2Pd_{1.25}Ge_{2.75}$ contains only ½ of the formula unit, resulting in VEC $= (2{\cdot}3 + 1.25{\cdot}0 + 2.75{\cdot}4)/2 = 8.5$ electrons/cell. Pd atoms are assumed to contribute 0 valence atoms due to the fact that the Pd contribution to the DOS (Fig. 11 (a) is almost completely contained between E = −6 and − 1 eV, consistent with Pd d^{10} closed shell configuration. The ordered YGa_2 and the disordered $Y_2Pd_{1.25}Ge_{2.75}$ are thus almost isoelectronic (completely isoelectronic for the 1:3 Pd:Ge ratio). $Y_2Pd_{1.25}Ge_{2.75}$ is thus produced by "diluting" the Ge sublattice of the hypothetical "YGe_2" compound (VEC = 11) to reduce the number of electrons and stabilize the AlB_2-type structure. The reported crystal structure of YGe_2 is of the α-$ThSi_2$ type, which is generally more stable than AlB_2 for higher electron counts, as discussed by Zheng and Hoffmann [48]. The same picture holds for Y_2PtGe_3 (= $YPt_{0.5}Ge_{1.5}$) and Y_2NiGe_3 (= $YNi_{0.5}Ge_{1.5}$), both being "diluted" variants of "YGe_2".

Table 2
Superconducting and normal-state parameters for $Y_2Pd_{1.25}Ge_{2.75}$.

Parameter	*Unit*	$Y_2Pd_{1.25}Ge_{2.75}$
T_c	K	2.72
$\mu_0H_{c1}(0)$	mT	2.7
$\mu_0H_{c2}(0)$	T	2.94(5)
$\mu_0H_c(0)$	mT	46
$\lambda_{e\text{-}p}$	-	0.58
$\xi_{GL}(0)$	Å	106
$\lambda_{GL}(0)$	Å	4820
κ_{GL}	-	45
γ	mJ mol^{-1} K^{-2}	5.0(5)
β	mJ mol^{-1} K^{-4}	1.09(4)
θ_D	K	220(3)
$\Delta C_p/\gamma T_c$	-	1.38
DOS(E_F)	eV f.u.$^{-1}$	1.34
RRR	-	1.1
dT_c/dp	K/GPa	-0.17

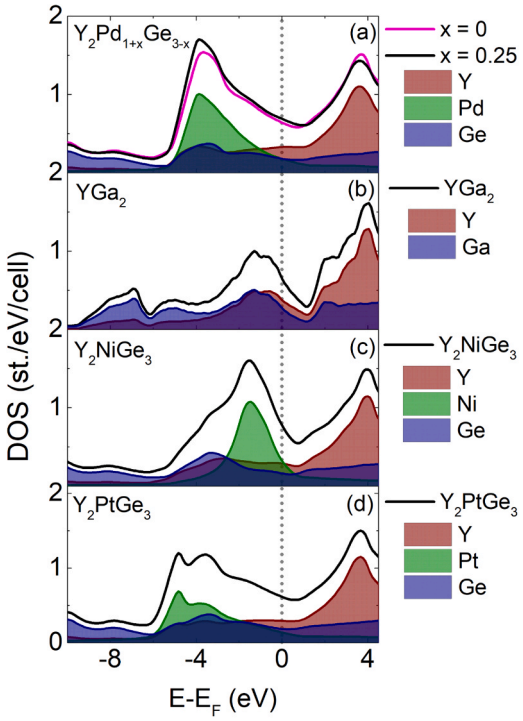

Fig. 11. Density of electronic states (DOS) calculated for $Y_2Pd_{1+x}Ge_{3-x}$ (x = 0 and 0.25; panel (a)), YGa_2 (b), Y_2NiGe_3 (c), and Y_2PtGe_3 (d). Altering the Pd:Ge ratio from 1:3–1.25:2.75 does not significantly affect the DOS around the Fermi level.

Quite often superconductivity arises at the verge of a structural distortion or charge density wave transition (see e.g. Refs. [49–52]). In a conventional superconductor the driving force behind the formation of Cooper pairs (necessary for the occurrence of superconductivity) is the interaction between electrons and atomic oscillations – electron-phonon coupling. However, the coupling between electronic and atomic motion is also responsible for the so-called softening of phonon modes, a hallmark of proximal structural distortion. In several systems, phonon structure calculations revealed the significant contribution of soft modes to the total electron-phonon coupling strength [53–57]. In case of $Y_2Pd_{1.25}Ge_{2.75}$ one can argue that the "d^{10}-dilution" of the Ge honeycomb sublattice of the hypothetical parent "YGe_2" allows to prevent a AlB_2 to α-$ThSi_2$ structural transition, however the tendency towards instability is not completely removed and results in an electron-phonon coupling strong enough to result in superconductivity. We recently discussed a similar behavior in $RbBi_2$ and $CsBi_2$ compounds, in which the distortion is prevented by strong relativistic effects, but the phonon structure shows softened modes that contribute significantly to the coupling strength [58].

4. Summary

A polycrystalline sample of a $Y_2Pd_{1.25}Ge_{2.75}$ intermetallic compound was synthesized via arc-melting technique. pXRD analysis confirms that the sample is single-phase. The electrical resistivity, heat capacity, and magnetic susceptibility measurements confirm bulk superconductivity with a $T_c \approx 2.7$ K. The compound is shown to be a weakly-coupled type-II superconductor, with $\lambda_{e\text{-}p} = 0.58$ and $\Delta C/\gamma T_c = 1.38$. A decrease of T_c is observed when increasing pressure is applied to the sample with a magnitude similar to observed in the related SrAlSi superconductor. DFT calculations reveal that electronic structure of $Y_2Pd_{1.25}Ge_{2.75}$ bears a close resemblance to the isostructural YGa_2 superconductor and the former compound can be considered a "Pd-diluted YGe_2" system, in which addition of the closed shell Pd d^{10} atoms tunes the valence

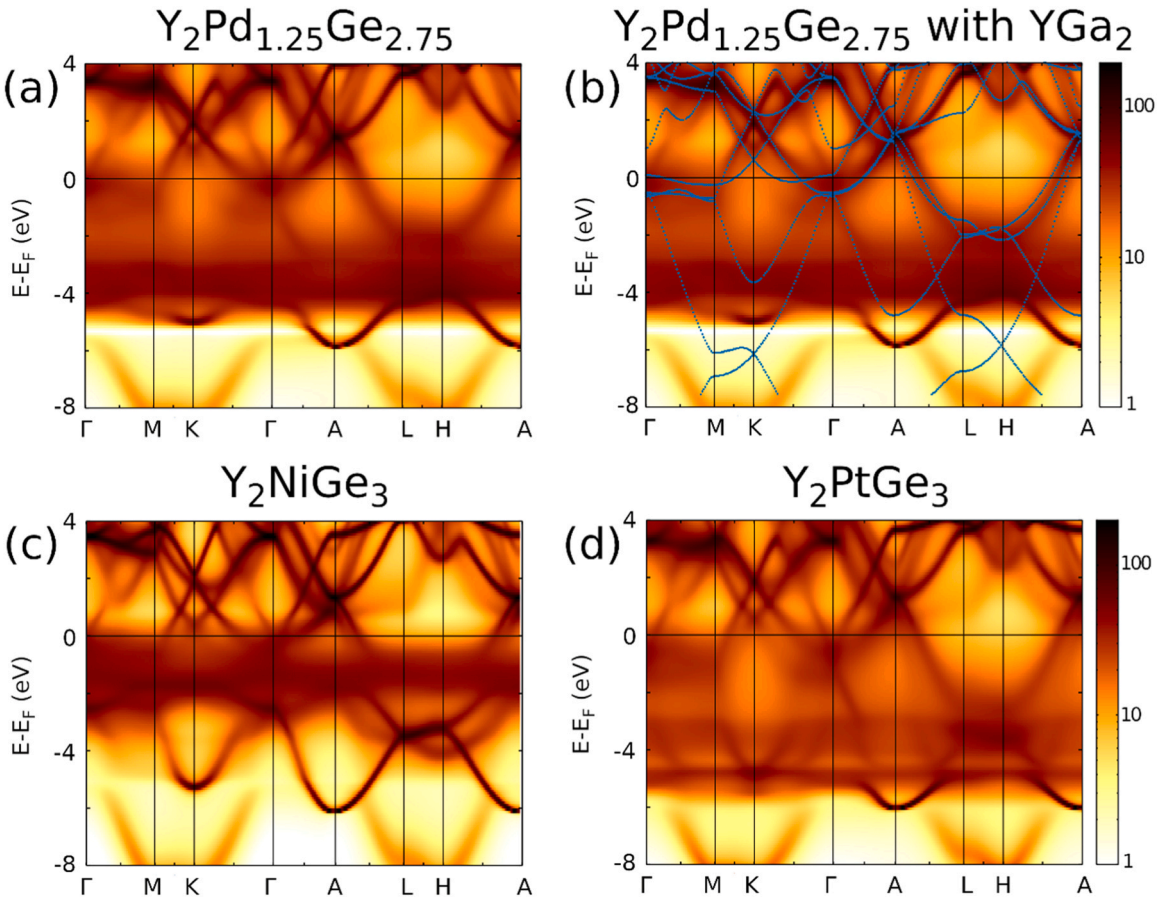

Fig. 12. Bloch spectral function (BSF) for (a,b) $YPd_{1.25}Ge_{2.75}$, (c) Y_2NiGe_3, (d) Y_2PtGe_3. Panel (b) shows the band structure of YGa_2 overlaid on BSF to highlight the similarity of electronic structures of the two compounds, especially around and above the Fermi level.

electron count to stabilize the AlB_2-type structure, while retaining a sizable electron-phonon coupling responsible for the emergence of superconductivity. The superconducting Ni- and Pt-bearing analogues were also found to show similar electronic structure.

CRediT authorship contribution statement

Hanna Świątek: Conceptualization, Investigation, Writing – original draft. **Szymon Królak:** Investigation. **Leszek Litzbarski:** Conceptualization, Resources. **Igor Oshchapovsky:** Investigation, Formal analysis. **Michał J. Winiarski:** Investigation, Formal analysis. **Tomasz Klimczuk:** Supervision, Visualization, Writing – review & editing.

Declaration of Competing Interest

The authors declare the following financial interests/personal relationships which may be considered as potential competing interests: Leszek Litzbarski reports financial support was provided by Ministry of Education and Science of the Republic of Poland.

Data availability

Data will be made available on request.

Acknowledgements

This paper was supported by the Ministry of Science and Higher Education (Poland) under Project No. DIA/2017/014247 ("Diamentowy Grant"). MJW gratefully acknowledges the Gdańsk Tech IDUB AURUM research grant program (project no. DEC-5/2020/IDUB/II.1.3). The authors would like to thank dr Karolina Górnicka for valuable discussions.

Appendix A. Supporting information

Supplementary data associated with this article can be found in the online version at doi:10.1016/j.jallcom.2023.172712.

References

[1] J. Nagamatsu, N. Nakagawa, T. Muranaka, Y. Zenitani, J. Akimitsu, "Superconductivity at 39 K in magnesium diboride, Nature vol. 410 (6824) (2001) 63–64, https://doi.org/10.1038/35065039.
[2] M. Tomsic, et al., "Overview of MgB2 superconductor applications, Int. J. Appl. Ceram. Technol. vol. 4 (3) (2007) 250–259, https://doi.org/10.1111/j.1744-7402.2007.02138.x.
[3] K. Vinod, R.G. Abhilash Kumar, U. Syamaprasad, Prospects for MgB2 superconductors for magnet application, Supercond. Sci. Technol. vol. 20 (1) (2007) R1, https://doi.org/10.1088/0953-2048/20/1/R01.
[4] D. Patel, et al., Superconducting joints using multifilament MgB2 wires for MRI application, Scr. Mater. vol. 204 (2021), 114156, https://doi.org/10.1016/j.scriptamat.2021.114156.
[5] X.X. Xi, Two-band superconductor magnesium diboride, Rep. Prog. Phys. vol. 71 (11) (2008), 116501, https://doi.org/10.1088/0034-4885/71/11/116501.
[6] R.-D. Hoffmann, R. Pöttgen, AlB2-related intermetallic compounds – a comprehensive view based on group-subgroup relations, Z. Für Krist. - Cryst. Mater. vol. 216 (3) (2001) 127–145, https://doi.org/10.1524/zkri.216.3.127.20327.
[7] T. Klimczuk, et al., Crystal structure and physical properties of new Ca2TGe3 (T = Pd and Pt) germanides, J. Solid State Chem. vol. 243 (2016) 95–100, https://doi.org/10.1016/j.jssc.2016.07.029.
[8] L.S. Litzbarski, M.J. Winiarski, P. Skokowski, T. Klimczuk, B. Andrzejewski, Investigation of magnetic order in a new intermetallic compound Nd2PtGe3, J. Magn. Magn. Mater. vol. 521 (2021), 167494, https://doi.org/10.1016/j.jmmm.2020.167494.

[9] C. Tien, C. Feng, C. Wur, J. Lu, Ce2CuGe3: A nonmagnetic atom-disorder spin glass, Phys. Rev. B vol. 61 (2000) 12158–74065, https://doi.org/10.1103/PhysRevB.61.12151.

[10] S. Pakhira, C. Mazumdar, R. Ranganathan, S. Giri, M. Avdeev, Large magnetic cooling power involving frustrated antiferromagnetic spin-glass state in R2NiSi3 (R=Gd,Er), Phys. Rev. B vol. 94 (10) (2016), 104414, https://doi.org/10.1103/PhysRevB.94.104414.

[11] H. Kito, Y. Takano, K. Togano, Superconductivity in ternary germanide Y (Pt0.5Ge1.5) with the AlB2-type structure, Phys. C. Supercond. vol. 377 (2002) 185–189, https://doi.org/10.1016/S0921-4534(02)01331-X.

[12] J.W. Chen, S.Y. Guan, C.H. Wang, S.P. Ho, Superconductivity of the Ni-based ternary compounds with AlB2-type structure Y2NiGe3 and La2NiGe3, Phys. C. Supercond. vol. 477 (2012) 63–65, https://doi.org/10.1016/j.physc.2012.02.028.

[13] S. Pakhira, C. Mazumdar, R. Ranganathan, Low-field induced large magnetocaloric effect in Tm2Ni0.93Si2.93: Influence of short-range magnetic correlation, J. Phys. Condens. Matter vol. 29 (2017), 505801, https://doi.org/10.1088/1361-648X/aa9736.

[14] J. Chen, N.S. Chou, N.R. G, F. Chou, Crystal structure, electrical, and magnetic properties of the Sm2Cu0.8Ge3 compound, Intermetallics vol. 54 (2014) 56–59, https://doi.org/10.1016/j.intermet.2014.05.009.

[15] K.J. Lin, et al., Modification of magnetic ground state in Tb2Ni0.90Si2.94 by thermal annealing, Z. Krist. vol. 224 (June) (1997) 42–44, https://doi.org/10.1524/zkri.2009.1115.

[16] L.S. Litzbarski, T. Klimczuk, M.J. Winiarski, Synthesis, structure and physical properties of new intermetallic spin glass-like compounds RE2PdGe3 (RE = Tb and Dy), J. Phys. Condens. Matter vol. 32 (22) (2020), 225706, https://doi.org/10.1088/1361-648X/ab73a4.

[17] L.S. Litzbarski, T. Klimczuk, M.J. Winiarski, Ho2Pd1.3Ge2.7 – a ternary AlB2-type cluster glass system, RSC Adv. vol. 11 (41) (2021) 25187–25193, https://doi.org/10.1039/D1RA04422B.

[18] L.S. Litzbarski, et al., Intermetallic disordered magnet ${\mathrm{Gd}}_{2}{\mathrm{Pt}}_{1.1}{\mathrm{Ge}}_{2.9}$ and its relation to other ${\mathrm{AlB}}_{2}$-type compounds, Phys. Rev. B vol. 105 (5) (2022) 54427, https://doi.org/10.1103/PhysRevB.105.054427.

[19] S. Majumdar, E.V. Sampathkumaran, Observation of enhanced magnetic transition temperature in Nd2PdGe3 and superconductivity in Y2PdGe3, Phys. Rev. B vol. 63 (17) (2001), 172407.

[20] E.V. Sampathkumaran, S. Majumdar, W. Schneider, S. Molodtsov, C. Laubschat, Superconductivity in Y2PdGe3, Phys. B Condens. Matter vol. s 312–313 (2002) 152–154, https://doi.org/10.1016/S0921-4526(01)01559-9.

[21] S. Takano, Y. Iriyama, Y. Kimishima, M. Uehara, Chemical substitution effects of Si and C on AlB2-type superconductor Y2PdGe3, Phys. C. Supercond. vol. 383 (4) (2003) 295–298, https://doi.org/10.1016/S0921-4534(02)02066-X.

[22] A. Ghosh, H. Nakamura, M. Tokunaga, T. Tamegai, Superconductivity in Y2PdGe3-xSix: Interplay between Debye temperature and coupling constant, Phys. C. -Supercond. Its Appl. - Phys. C. vol. 388 (2003) 567–568, https://doi.org/10.1016/S0921-4534(02)02743-0.

[23] K.K. Iyer, E.V. Sampathkumaran, Superconducting behavior of the solid solution, Y2Pd1−xPtxGe3, Phys. C. Supercond. vol. 466 (1) (2007) 51–55, https://doi.org/10.1016/j.physc.2007.05.049.

[24] A.R. Denton, N.W. Ashcroft, Vegard's law, Phys. Rev. A vol. 43 (6) (1991) 3161–3164, https://doi.org/10.1103/PhysRevA.43.3161.

[25] A.A.R. Fernandes, J. Santamaria, S.L. Bud'ko, O. Nakamura, J. Guimpel, I. K. Schuller, Effect of physical and chemical pressure on the superconductivity of high-temperature oxide superconductors, Phys. Rev. B vol. 44 (14) (1991) 7601–7606, https://doi.org/10.1103/PhysRevB.44.7601.

[26] Y. Mizuguchi, et al., In-plane chemical pressure essential for superconductivity in BiCh2-based (Ch: S, Se) layered structure, Sci. Rep. vol. 5 (1) (2015) 14968, https://doi.org/10.1038/srep14968.

[27] V. Petříček, M. Dušek, L. Palatinus, Crystallographic Computing System JANA2006: General features, Z. Für Krist. - Cryst. Mater. vol. 229 (5) (2014) 345–352, https://doi.org/10.1515/zkri-2014-1737.

[28] M.J. Clark, T.F. Smith, Pressure dependence of Tc for lead, J. Low. Temp. Phys. vol. 32 (3) (1978) 495–503, https://doi.org/10.1007/BF00117966.

[29] H. Ebert, D. Ködderitzsch, J. Minár, Calculating condensed matter properties using the KKR-Green's function method—recent developments and applications, Rep. Prog. Phys. vol. 74 (9) (2011), 096501, https://doi.org/10.1088/0034-4885/74/9/096501.

[30] J.P. Perdew, K. Burke, M. Ernzerhof, Generalized gradient approximation made simple, Phys. Rev. Lett. vol. 77 (18) (1996) 3865–3868, https://doi.org/10.1103/PhysRevLett.77.3865.

[31] D. Rossi, R. Ferro, Ternary rare earth (R) alloys occurring in some ~RPd2−xGex sections, Intermetallics vol. 10 (4) (2002) 399–402, https://doi.org/10.1016/S0966-9795(02)00002-X.

[32] L. Palatinus, G. Chapuis, SUPERFLIP – a computer program for the solution of crystal structures by charge flipping in arbitrary dimensions, J. Appl. Crystallogr. vol. 40 (4) (2007) 786–790, https://doi.org/10.1107/S0021889807029238.

[33] C.R. Rotundu, V.V. Struzhkin, M.S. Somayazulu, S. Sinogeikin, R.J. Hemley, R. L. Greene, High-pressure effects on single crystals of electron-doped Pr 2 − x Ce x CuO 4, Phys. Rev. B vol. 87 (2) (2013), 024506, https://doi.org/10.1103/PhysRevB.87.024506.

[34] T. Klimczuk, T. Plackowski, W. Sadowski, M. Plebańczyk, A resistivity peak close to Tc in Nd2−xCexCuO4−y single crystals, Phys. C. Supercond. vol. 387 (1–2) (2003) 203–207, https://doi.org/10.1016/S0921-4534(03)00670-1.

[35] M.R. van Delft, S. Pezzini, M. König, P. Tinnemans, N.E. Hussey, S. Wiedmann, Two- and Three-Dimensional Superconducting Phases in the Weyl Semimetal TaP at Ambient Pressure, Crystals vol. 10 (4) (2020) 288, https://doi.org/10.3390/cryst10040288.

[36] R. Micnas, J. Ranninger, S. Robaszkiewicz, Superconductivity in narrow-band systems with local nonretarded attractive interactions, Rev. Mod. Phys. vol. 62 (1) (1990) 113–171, https://doi.org/10.1103/RevModPhys.62.113.

[37] Z. Ryżyńska, et al., RuAl $_6$ —an endohedral aluminide superconductor, Chem. Mater. vol. 32 (9) (2020) 3805–3812, https://doi.org/10.1021/acs.chemmater.9b05277.

[38] L.C. Srivichitranond, E.M. Seibel, W. Xie, Z. Sobczak, T. Klimczuk, R.J. Cava, Superconductivity in a new intermetallic structure type based on endohedral Ta @ I r 7 G e 4 clusters, Phys. Rev. B vol. 95 (17) (2017), 174521, https://doi.org/10.1103/PhysRevB.95.174521.

[39] K. Inoue, et al., Superconductivity in BaCuxSi2-x ($0.2 \leq x \leq 0.6$) with AlB2-type structure, Phys. Procedia vol. 27 (2012) 52–55, https://doi.org/10.1016/j.phpro.2012.03.408.

[40] T. Klimczuk, M. Szlawska, D. Kaczorowski, J.R. O'Brien, D.J. Safarik, Superconductivity in the Einstein solid V Al10.1, J. Phys. Condens. Matter vol. 24 (36) (2012), 365701, https://doi.org/10.1088/0953-8984/24/36/365701.

[41] V.H. Tran, M. Sahakyan, Z. Bukowski, Discovery of superconductivity in AlB2-type hexagonal YGa2, J. Phys. Condens. Matter vol. 33 (31) (2021), 315401, https://doi.org/10.1088/1361-648X/ac02e3.

[42] W.L. McMillan, Transition temperature of strong-coupled superconductors, Phys. Rev. vol. 167 (2) (1968) 331–344, https://doi.org/10.1103/PhysRev.167.331.

[43] T. Klimczuk, R.J. Cava, Carbon isotope effect in superconducting Mg C Ni 3, Phys. Rev. B vol. 70 (21) (2004), 212514, https://doi.org/10.1103/PhysRevB.70.212514.

[44] B. Lorenz, J. Cmaidalka, R.L. Meng, C.W. Chu, Thermodynamic properties and pressure effect on the superconductivity in CaAlSi and SrAlSi, Phys. Rev. B vol. 68 (1) (2003), 014512, https://doi.org/10.1103/PhysRevB.68.014512.

[45] S. Kuroiwa, T. Kakiuchi, H. Sagayama, H. Sawa, J. Akimitsu, Quasi-two-dimensional superconducting characteristics in single-crystalline SrAlSi without superstructure, Phys. C. Supercond. Its Appl. vol. 460–462 (2007) 154–155, https://doi.org/10.1016/j.physc.2007.04.005.

[46] M.J. Winiarski, et al., Mg Pd 2 Sb: A Mg-based Heusler-type superconductor, Phys. Rev. B vol. 103 (21) (2021), 214501, https://doi.org/10.1103/PhysRevB.103.214501.

[47] G. Schadler, P. Weinberger, A. Gonis, J. Klima, Bloch spectral functions for complex lattices: applications to substoichiometric TiNx and the Fermi surface of TiNx, J. Phys. F. Met. Phys. vol. 15 (8) (1985) 1675, https://doi.org/10.1088/0305-4608/15/8/007.

[48] C. Zheng, R. Hoffmann, Conjugation in the 3-connected net: the aluminum diboride and thorium disilicide structures and their transition-metal derivatives, Inorg. Chem. vol. 28 (6) (1989) 1074–1080, https://doi.org/10.1021/ic00305a015.

[49] D. Sun, et al., High-temperature superconductivity on the verge of a structural instability in lanthanum superhydride, Art. no. 1, Nat. Commun. vol. 12 (1) (2021), https://doi.org/10.1038/s41467-021-26706-w.

[50] A. Kiswandhi, et al., Competition between the structural phase transition and superconductivity in Ir$_{1\ensuremath{-}x}$Pt$_{x}$Te$_{2}$ as revealed by pressure effects, Phys. Rev. B vol. 87 (12) (2013), 121107, https://doi.org/10.1103/PhysRevB.87.121107.

[51] O. Degtyareva, et al., Competition of Charge-Density Waves and Superconductivity in Sulfur, Phys. Rev. Lett. vol. 99 (15) (2007), 155505, https://doi.org/10.1103/PhysRevLett.99.155505.

[52] M. Kang, et al., Charge order landscape and competition with superconductivity in kagome metals, Art. no. 2, Nat. Mater. vol. 22 (2) (2023), https://doi.org/10.1038/s41563-022-01375-2.

[53] K. Górnicka, et al., Soft-mode enhanced type-I superconductivity in $\mathrm{Li}{\mathrm{Pd}}_{2}\mathrm{Ge}$, Phys. Rev. B 102 (2) (2020), 024507 https://doi.org/10.1103/PhysRevB.102.024507.

[54] M. Maschek, et al., Superconductivity and hybrid soft modes in $\mathrm{Ti}{\mathrm{Se}}_{2}$, Phys. Rev. B vol. 94 (21) (2016), 214507 https://doi.org/10.1103/PhysRevB.94.214507.

[55] S. Kuroiwa, A.Q.R. Baron, T. Muranaka, R. Heid, K.-P. Bohnen, J. Akimitsu, Soft-phonon-driven superconductivity in CaAlSi as seen by inelastic x-ray scattering, Phys. Rev. B vol. 77 (14) (2008), 140503, https://doi.org/10.1103/PhysRevB.77.140503.

[56] R. Lortz, et al., Superconductivity mediated by a soft phonon mode: Specific heat, resistivity, thermal expansion, and magnetization of YB6, Phys. Rev. B vol. 73 (2) (2006), 024512, https://doi.org/10.1103/PhysRevB.73.024512.

[57] X.-J. Chen, Exploring high-temperature superconductivity in hard matter close to structural instability, Matter Radiat. Extrem. vol. 5 (6) (2020), 068102, https://doi.org/10.1063/5.0033143.

[58] S. Gutowska, B. Wiendlocha, T. Klimczuk, M.J. Winiarski, Superconductivity in bismuth perochlore lattice compounds RbBi2 and CsBi2: the role of relativistic effects, J. Phys. Chem. C. vol. 127 (29) (2023) 14402–14414, https://doi.org/10.1021/acs.jpcc.3c02176.

[59] H. Ebert, et al., The Munich SPR-KKR package. version 8.6. https://www.ebert.cup.uni-muenchen.de/sprkkr.